Chinese Journal of Polymer Science Vol. 33, No. 1, (2015), 95–108

Chinese Journal of Polymer Science
© Chinese Chemical Society
Institute of Chemistry, CAS
Springer-Verlag Berlin Heidelberg 2015

Effects of Composition on Microstructure and Crystallization Behavior for Impact Polypropylene Copolymer Investigated by Restructuring the Complex Core-Shell Dispersed Particles in Ternary Blends*

Bi-wei Qiu, Feng Chen, Yong-gang Shangguan**, Yu Lin and Qiang Zheng**
MOE Key Laboratory of Macromolecular Synthesis and Functionalization, Department of Polymer Science and Engineering, Zhejiang University, Hangzhou 310027, China

Abstract A series of ternary blends of polypropylene/ethylene-propylene random copolymer/ethylene-propylene segmented copolymer (HPP/EPR/E*b*P) whose microstructures are similar to those of impact polypropylene copolymer (IPC) were prepared in order to systematically investigate the effects of composition on microstructure and crystallization behavior of IPC. The observation of primary phase morphology reveals that the dispersed phase with core-shell structure could be rebuilt in certain composition and excessive EPR leads to a bicontinuous phase structure in ternary blends. After undergoing same quiescent crystallization including isothermal and non-isothermal crystallization, these blend samples exhibit special composition-dependent melting behavior, *i.e.*, the melting point increases markedly with the increase of EPR content until it turns down at a critical content (about 30 wt%). The crystallization behavior is mainly ascribed to the different nucleation abilities. It is suggested that although the compatibility between EPR and HPP components becomes worse with the increase of EPR content due to the increased interfacial area and the decreased concentration of E*b*P, higher EPR content in the blend facilitates to heterogeneous nucleation except for the appearance of obvious bicontinuous phase structure.

Keywords: Core-shell dispersed phase; Microstrcture; Crystallization; Nucleation.

Electronic Supplementary Material Supplementary material is available in the online version of this article at http://dx.doi.org/10.1007/s10118-015-1556-8.

INTRODUCTION

It is well known that impact polypropylene copolymer (IPC), synthesized *via* a continuous polymerization system with propylene and ethylene in a gas-phase reactor, has been proved to own excellent impact property[1–4] by drawing compositional heterogeneity propylene-ethylene copolymer (ethylene-propylene random copolymer (EPR) and ethylene-propylene segmented copolymer (E*b*P))[4–6] into propylene homopolymer (HPP) matrix. The attractive properties are thought to stem from its complex composition and microstructure as well as the crystallization behavior of HPP matrix[4, 7–11]. Since microstructure and crystallization of multi-component systems usually strongly depend on composition[12, 13], it is necessary to investigate the effects of composition on them. However, few systemic investigations about these in IPC have been reported as it is difficult to obtain the IPC samples with regular changing in composition by copolymerization.

* This work was financially supported by the National Natural Science Foundation of China (Nos. 51173157 and 51173165), the Fundamental Research Funds for the Central Universities (No. 2013QNA4048) and Nature Science Foundation of Zhejiang Province (No. Y4100314).
** Corresponding authors: Qiang Zheng (郑强), E-mail: zhengqiang@zju.edu.cn
Yong-gang Shangguan (上官勇刚), E-mail: shangguan@zju.edu.cn
Received April 3, 2014; Revised May 29, 2014; Accepted July 2, 2014
doi: 10.1007/s10118-015-1556-8

The complicated heterogeneous morphology of IPC results from the coexistence of EPR and E*b*P as dispersed domains in the HPP matrix[5, 14]. In addition, it is considerable that the effect of composition on phase structure (shape, size and distribution of dispersed phase) is related to the miscibility between components. In the case of IPC, the HPP and EPR components are immiscible and E*b*P is proved to be a good compatibilizer to them[5]. Kock *et al*.[14] proposed that better compatibility allowed the development of multiphase materials with finer phase structure because of little interfacial tension. Fu *et al*.[15] found that the alloy presented smaller and more uniform dispersed rubber phase in the presence of a good compatibilizer.

For amorphous/crystallizable blends, primary phase morphology can usually influence the crystallization behavior and subsequent crystalline structure of the crystallizable component. Although the composition may simultaneously affect the nucleation and crystal growth, in most situations the effect on crystallization behavior was reported to be dominated by nucleation (including nuclei density and nucleation rate). The nucleation efficiency is usually related to the compatibility, interfacial area and even the concentration fluctuation during liquid-liquid phase separation (LLPS), which are all dependent on the composition. In the case of a miscible PP blend, the nucleation of PP spherulite is greatly depressed by the dilution effect of amorphous components[16, 17]. But for partial miscible or immiscible PP blends[18–21], the nucleation is enhanced by heterogonous nucleation effect. Jin *et al*.[22] believed that the nucleation easily happened in the blends with better compatibility, and this enhancement of nucleation could be depressed by imposing a macroscopic phase separation process before crystallization in *i*PP/OBC (isotactic polypropylene/polyolefin block copolymers) blends. The interplay between the nucleation and LLPS in the polymer melt has also been investigated recently[23–26]. Tsuburaya *et al*.[24] attributed the accelerated nucleation behavior to the up-hill diffusion of LLPS *via* spinodal decomposition. Han and his coworkers[25, 26] contended that the increased nucleation rate resulted from the chain segmental alignment induced by the concentration fluctuation at the early stage of phase separation, and it was proportional to the interfacial area at later phases coarsening process. Similarly, melting behavior of PP blends also exhibits composition dependence. The addition of elastomer could decrease melting temperatures which may result from disturbing the regularity of spherulite by the elastomer localized in intra-spherulitic regions[27] while Martuscelli *et al*.[18] observed the elevation of melting point in *i*PP/EPM (random ethylene-propylene copolymer) blends. In a word, there is no unifying understanding of the composition dependence of crystallization behavior.

As mentioned above, although there have some literatures on the study of microstructure, morphology, crystallization and properties of multiphase blends, a systemic understanding on the effects of composition on microstructure and crystallization of IPC is still urgent. Our previous works tried to regulate composition by changing content of propylene and ethylene in sequential polymerization[6, 13, 20], but the actual composition is much complex so that it is inconvenient to adjust regularly. Fortunately, it was reported that a HPP/EPR/E*b*P ternary blend prepared by solution-mixing could present a same phase structure as original IPC[28], indicating that the special phase structure of IPC could be restructured in certain conditions. Therefore, in this work, we try to conduct a two-step sample preparation by temperature-gradient extraction fractionation (TGEF) and subsequent solution-mixing in order to obtain the ternary HPP/EPR/E*b*P blends with different compositions. Subsequently, we focus on the influences of composition on the microstructure and crystallization behavior of the ternary blends and in particular, analyze crystalline structure and crystallization kinetics on the basis of the Thomson-Gibbs, Scherrer equations and Lauritzen-Hoffman model respectively.

EXPERIMENTAL

Materials and Sample Preparation

A commercial IPC (SP179) purchased from Sinopec Qilu Petrochemical Co. of China was used to extract fractions and prepare blend samples. According to TGEF method, IPC was first completely dissolved in boiling *n*-octane at 125 °C and then cooled down to 50 °C to isolate the solution (F50) from insoluble substance. After adding adequate *n*-octane into insoluble substance, the solution was heated to 100 °C for 72 h so that the insoluble fraction was dissolved partly again and newly solvable fraction (F100) with solution temperatures from

50 to 100 °C was collected. After distillation and drying of rest solution, the final insoluble substance (F125) was also obtained. Component analysis suggested that the fractions of EPR (F50), segmented copolymer E*b*P (F100) and HPP (F125) correspond to the solvable substances with solution temperature of 50 °C, 100 °C and 125 °C respectively[4, 5, 29]. The melting curves of the three fractions as showed in Fig. 1 certify the components further: i) almost no endothermic peak exists in F50, ii) two peaks of F100 correspond to melting of PE and PP crystals respectively, and iii) double peaks in F125 both belong to PP. The molecular weight and its distribution for IPC and fractions are listed in Table 1.

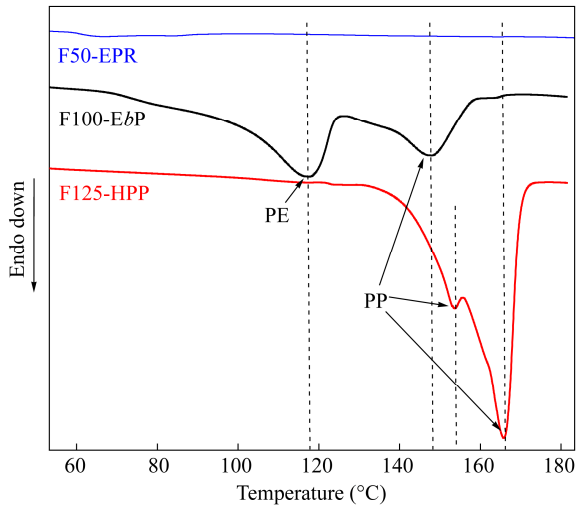


Fig. 1 Endotherms of the three fractions extracted from IPC

Table 1. Molecular weight and molecular weight distribution for IPC and its fractions*

Sample	$M_w \times 10^{-4}$	M_w/M_n*
IPC	17.4	3.96
HPP (69%)	9.34	2.84
EPR (21%)	36.1	3.16
E*b*P (10%)	4.25	4.48

* Determined by gel permeation chromatography (GPC)

The HPP/EPR/E*b*P blends were prepared by solution-mixing. Three fractions with designated weight ratio were first dissolved in boiling xylene successively. After completely mixing for about 30 min, the blend was precipitated in excessive methanol. Through filtrating and drying the precipitant for 72 h, HPP/EPR/E*b*P blends with four compositions (60/30/10, 69/21/10, 80/10/10 and 90/0/10 in weight) were prepared. Here, the content of EbP is fixed in all blends and in particular, composition of 69/21/10 (HPP/EPR/EbP) is the same as the original IPC.

Scanning Electron Microscope (SEM) Observation

The blend samples were quickly quenched and fractured in liquid nitrogen after being compressed at 190 °C. They were adequately etched in xylene for 4 h at 52 °C to remove amorphous EPR and sputter-coated with gold powder, then the fractured surface of the samples was observed by SEM (SIRION, FEI, Netherland).

Differential Scanning Calorimetry (DSC) Analysis

A DSC (Q100, TA Instruments Corporation) instrument with nitrogen as purge gas was used to probe crystallization and melting behavior. The isothermal crystallization and non-isothermal crystallization (cooling rates of 2 and 10 K/min) were adopted, respectively. The weight of each sample was kept at (6 ± 0.5) mg. All blends were heated to 210 °C and held for 10 min to eliminate thermal history firstly. After crystallization, the samples were heated to 200 °C at a rate of 10 K/min again to record the melting trace.

Optical Microscope Observation

Polarized optical microscopy (POM) and phase contrast optical microscopy (PCM) observations were carried out using an optical microscope (BX51, Olympus) equipped with an Olympus camera and a temperature controlled hot stage (THMS600, Linkam Co). The specimens were sandwiched to about 10 μm between two microscope cover slips for observation.

Wide-angle X-ray Diffraction (WAXD) Analysis

WAXD patterns of the film samples were obtained on a D/Max-2550PC X-ray diffractometer with the Cu Kα radiation at room temperature. The wavelength (λ) of the X-ray beam was 0.154059 nm. In this study, the continuous scanning angle (2θ) ranged from 3° to 40° at a voltage of 40 kV and a current of 250 mA. The *d*-spacing of the sample was scanned at 5 (°)/min, with a step of 0.02°.

RESULTS AND DISCUSSION

Phase Morphology

In present work, the amount of E*b*P component in all blend samples is fixed and the weight ratio of HPP/EPR monotonously changes. As shown in Fig. 2, an obvious multiphase structure can be observed after removing the EPR dispersed phase through etching of xylene. The holes represent the removed EPR component, and the particles inside (Fig. 2b) or hanging along interphase (Fig. 2c) are the E*b*P component (because the inclusions disappear after being etched in xylene at 100 °C as shown by inserted image in Fig. 2(b) but they couldn't be dissolved in xylene at 52 °C) while the rest is chiefly HPP matrix[5]. Note that the EPR component in blends was extracted from IPC in *n*-octane at 50 °C, it could be dissolved completely in xylene at a higher temperature (the *n*-octane and xylene have similar solubility to EPR[30]). It has been proved that the great viscosity difference and good compatibility between EPR and E*b*P component result in the special dispersed phase consisted of EPR and E*b*P in IPC[5, 8]. For the dispersed phase, the core-shell structure is composed of an E*b*P core (with long ethylene chain segment) and two shells, the outer E*b*P layer (with long propylene chain segment) and the inner EPR one[5, 31, 32]. Here, the EPR shell could be observed clearly by etching while the outer E*b*P shell, located at the interface, is difficult to define by SEM. Nevertheless, E*b*P shell is closely related to the state of interface between HPP matrix and dispersed phase.

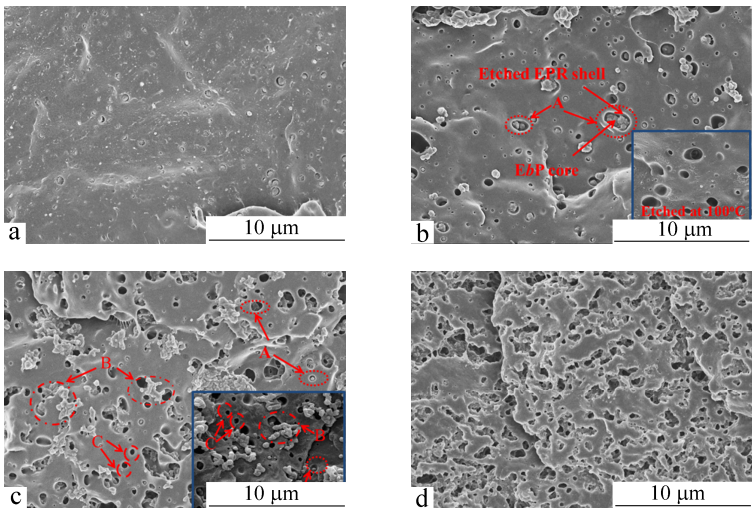


Fig. 2 SEM micrographs of HPP/EPR/E*b*P blends of different compositions, etched by xylene at 52 °C: (a) 90/0/10, (b) 80/10/10. (c) 69/21/10 and (d) 60/30/10 (The inserted image in (b) shows micrograph after etching at 100 °C, and the inserted image in (c) is for IPC.)

Figure 2(c) shows phase morphology of the blend which has a same composition as original IPC and the dispersed phase with core-shell structure is definitely indicated by arrows. The extreme similarity suggests that the core-shell dispersed phase has been rebuilt in the ternary blend and that it is feasible for the blends to represent IPC to some extent. It is seen that the phase structure greatly varies with the composition. For the HPP/EPR/E*b*P (90/0/10) blend without EPR component, few was etched by xylene at 52 °C except some short E*b*P chains, so dispersed particles with small size only consisting of E*b*P emerge indistinctly. With the increase of EPR content, the sizes of dispersed particles enlarge. In the case of HPP/EPR/E*b*P (80/10/10) blend, the dispersed phase presents the typical core-shell structure (labelled by 'A'). As the content of EPR increases to 21 wt%, dispersed particles with thicker EPR shell (labelled by 'B') increase and it is easy to bring E*b*P core out. Meanwhile, spherical dispersed phases without visible cores (labelled by 'C') increase. Because part of excessive EPR component encapsulates E*b*P core completely or disperses separately so that some dispersed particles could be moved away thoroughly by etching. Further increasing the EPR content, only some irregularly semicontinuous and continuous holes exist in HPP/EPR/E*b*P (60/30/10) blend, indicating that an almost continuous network has been built.

As a compatibilizer, E*b*P could improve interfacial interaction and help to refine the dispersed phase. Previous literatures[1, 2] indicated that PP-rich E*b*P component located between HPP and EPR phases. The great concentration of E*b*P at the interfacial location facilitates improving compatibility. Thus, the outer E*b*P shell could be detected indirectly by the state of interphase. The E*b*P content of four blends keeps identical, but the E*b*P concentration at interface is indeed different so that the compatibility between HPP and EPR phases is different too. Due to the increased interfacial area, the decrease of average concentration of E*b*P in interfacial location is considerable, so the compatibility becomes worse with the increase of EPR content. As a result, the domains of the dispersed phase with weak interfacial adhesion could be easily removed from matrix while the ones with strong interaction are firmly limited. These results also indicate that the dispersed particles with complex core-shell structure in IPC only occur in ceratin compositions and excessive EPR component will lead to an obvious bicontinuous phase structure.

Crystallization and Melting Behavior

To probe effects of the composition on crystallization and subsequent melting behavior, the quiescent crystallization behavior (isothermal and non-isothermal crystallization) and melting behavior as well as crystalline structure of ternary blends were investigated as following.

Given that the crystallization and melting behavior of ternary blends show the similar temperature and composition dependences, we choose the HPP/EPR/E*b*P (69/21/10) blend to demonstrate the temperature dependence and the composition dependence at a given temperature, as shown in Fig. 3. Under the same condition, the crystallization time extends with elevated temperature, but it shortens with increasing content of EPR until a reverse happens for HPP/EPR/E*b*P (60/30/10) with excessive EPR. The half crystallization time ($t_{1/2}$), corresponding to the time at a relative degree of crystallinity of 50%, is used to evaluate the crystallization rate. At arbitrary crystallization temperatures under this investigation, the $t_{1/2}$ decreases as EPR content increases and an exception appears when EPR content reaches 30 wt%. In other words, the overall crystallization rate G^* increases with the increase of EPR content until a distinct decrease takes place for HPP/EPR/E*b*P(60/30/10). Considering that the crystallization of polymeric materials is usually determined by two terms: nucleation and growth, so the difference of crystallization rate among ternary blends may lie in different nucleation behavior or crystal growth rate. The reason would be explored in next section.

In the case of melting behavior, with the increase of EPR content, the melting peak obviously shifts toward high temperature and then turns down for the HPP/EPR/E*b*P(60/30/10) blend. However, we found that the calculated equilibrium melting temperatures (T_m^0) of HPP crystal in the blends by Gibbs Thomson equation[33] are similar, as given in Fig. S1 in Supporting Information, and consequently a T_m^0 of 194.61 °C is applied for all blends. Here, the calculated T_m^0 is slightly larger than that in literatures[34, 35], which may be ascribed to the nucleation effect of dispersed phase.

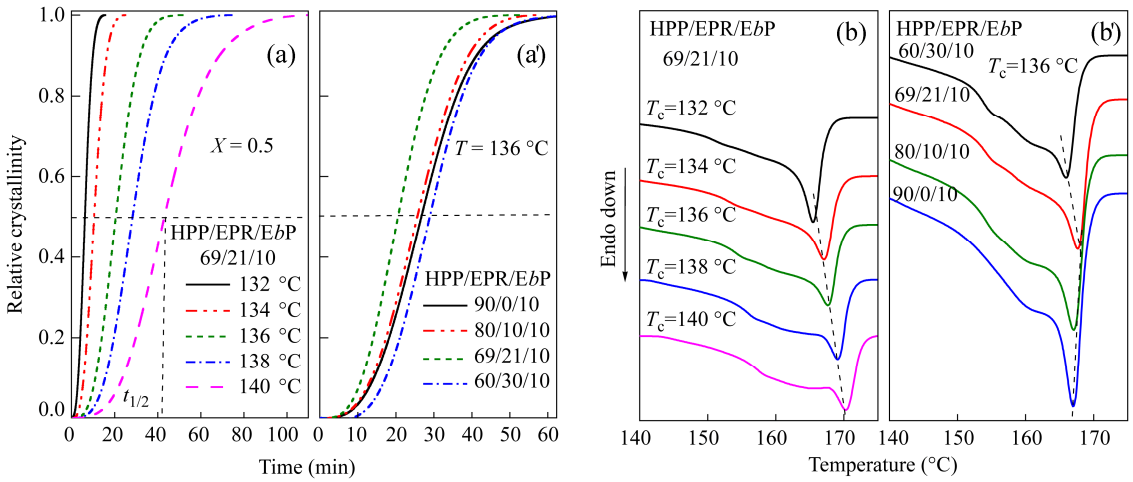


Fig. 3 The relative crystallinity versus time (a) (a') and corresponding endotherms (b) (b') for HPP/EPR/E*b*P blends and at different isothermal crystallization temperatures

According to the modified Gibbs-Thomson equation[36, 37], the correlation between melting points and lamellar thickness (L_c) can be described as following:

$$L_c = \frac{2\sigma_e T_m^0 \Delta z}{\Delta h_f^0 (T_m^0 - T_m)} \quad (1)$$

where σ_e is the free energy for folding surface, Δz is the length of three folded monomer units (helical structure, Δz = 0.65 nm)[38], Δh_f is the heat of fusion per unit volume (166.608 J/cm^3 for HPP[13]), and T_m^0 and T_m are equilibrium melting point and melting point respectively. The calculated lamellar thicknesses are listed in Table 2. The results show that mean lamellar thickness increases with increasing of EPR content, but a smaller value appears when the EPR content reaches 30 wt%.

Table 2. Crystalline parameters for HPP/EPR/E*b*P blends

Samples	DSC (L_c, nm)					WAXD	
	132 °C	134 °C	136 °C	138 °C	140 °C	β_{110} (°)	D_{110} (nm)
90/0/10	11.06	11.54	11.90	12.30	12.87	0.425	19.02
80/10/10	11.22	11.64	11.93	12.64	13.07	0.418	19.38
69/21/10	11.68	11.94	12.65	12.89	13.47	0.405	19.99
60/30/10	10.76	10.92	11.46	12.16	12.28	0.399	20.29

The melting temperature usually keeps identical for a polymer crystallized at certain condition[13, 39]. But in a thermodynamic viewpoint, there is always a tendency for the thinner lamellae to rearrange into more stable state, *i.e.*, lamellae thickening above its glass transition temperature[40]. Liu *et al.*[41] proposed that the main lamellar thickening is nucleation-controlled, as a bundle-like nucleus of thickened domain could form and grow further after an incubation period of chain unfolding. Here, heterogeneous nucleation is the major nucleation mode (indicated by the calculated Avrami exponent in Table S1 of Supporting Information). Therefore, the difference of lamellar thickness should be ascribed to the different nucleation ability induced by distinct phase structure. Usually, under the same isothermal crystallization condition the earlier the nucleation completes, the longer the time for lamella thickening. Note that the primary phase structure is dependent on EPR concentration in matrix. As mentioned previously, although the increasing EPR content could lead to a lower E*b*P concentration in interfacial location and consequently reduce the compatibility between EPR and HPP components in blend samples, the EPR amount in HPP-rich phase may increase until it aggregates greatly and the HPP approaches neat component. In addition, the introduction of E*b*P into lamellae would affect the crystal

perfection and in turn decrease the lamellae thickness, compared with pure HPP. However, for the blends, the influence of heterogeneous nucleation on lamellae thickness may be larger than that of the introduction of the irregular chain, so the melting temperature increases with the increase of EPR content. Here, the nucleation ability of the dispersed phase is simultaneously influenced by compatibility and the content of heterogeneous component in HPP-rich phase. Based on above discussions, we can conclude that the nucleation ability increases when the EPR content increases from 0% to 21%. Contrarily, when the EPR content reaches 30%, the too poor compatibility results in the appearance of bicontinuous phase structure and consequently eliminates the nucleation. The different nucleation abilities of the four ternary blend samples will be affirmed by the non-isothermal crystallization experimental results. Thus, with the increase of EPR content, the melting temperature of blend samples shows a general increase before the final drop.

It is considerable that the primary phase structure could also affect spherulite structure[42]. Figure 4 shows the POM and corresponding PCM micrographs of spherulites isothermally crystallized at 140 °C. It can be found that the blend sample with composition of 90/0/10 exhibits a regular Maltese-cross, indicating the E*b*P is involved in the crystallization of HPP. With increasing EPR content, the Maltese-cross pattern of HPP spherulites becomes indistinct and diffused gradually. Since spherulite is optically anisotropic and birefringent, the diffused Maltese-cross can be ascribed to the increase of interfibrill amorphous phase and inhomogeneity in spherulites. Considering that the HPP/EPR blend is indeed immiscible at melt state[5], it can be observed that micro domains inside spherulites generally increase and boundaries of interphase become significant with the increase of EPR content at 140 °C.

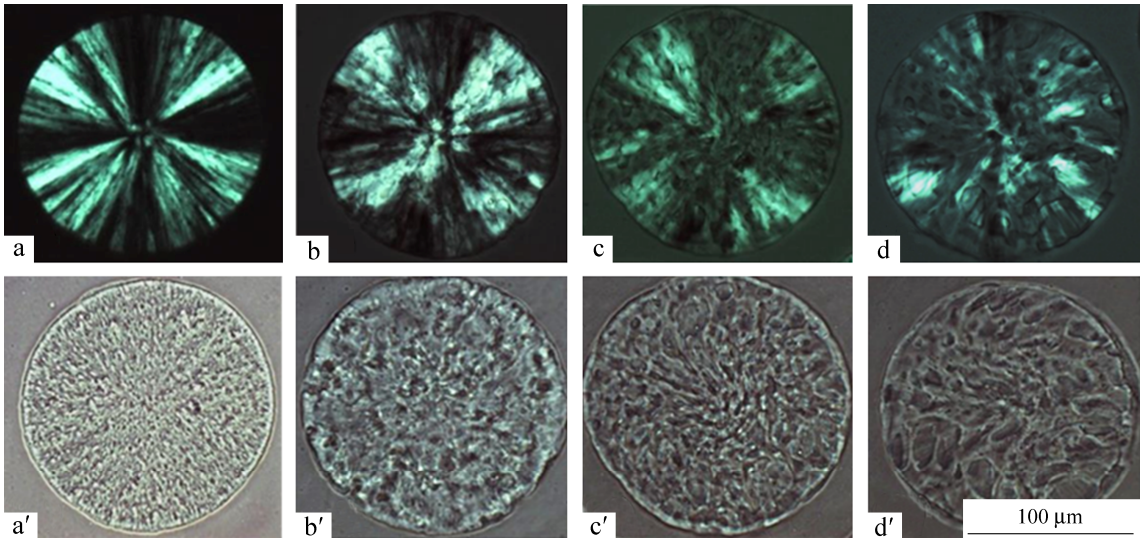


Fig. 4 POM (a)–(d) and corresponding PCM (a')–(d') morphology of HPP/EPR/E*b*P blends with different compositions crystallized at 140 °C: (a) (a') 90/0/10, (b) (b') 80/10/10, (c) (c') 69/21/10 and (d) (d') 60/30/10

Generally speaking, lower melting temperature is thought to correspond to smaller lamella thickness or imperfect crystals whereas higher melting temperature indicates the melting of perfect crystals[43]. Since the melting temperature is directly correlated with lamella thickness, the above results in Fig. 4 only indicate the disagreement between lamella thickness and spherulite perfection in these ternary blends. Actually, the Maltese-cross pattern of spherulites reflects homogeneity of crystalline region in macro-scale. Hence it is more reasonable to evaluate crystal by microstructure of lamellae, but macroscopic structure of spherulite.

The DSC curves of non-isothermal crystallization and melting behavior of blend samples are shown in Fig. 5. Two cooling rates were adapted to distinguish the effects of composition on crystallization and melting behavior. It is found that these blends present similar composition dependences. As well known, the onset

temperature during crystallization could reflect nucleation ability in some degree. The results show that the nucleation of HPP is delayed and the melting points are depressed after adding both E*b*P and EPR components, especially only mixed with E*b*P. Those are ascribed to homogeneous distribution of various kinds of molecular chains by solution mixing and determined by compatibility of components. Good compatibility allows a fine mixing of chains while poor compatibility may cause phase separation and coarsening easily. The onset temperature of crystallization rises as EPR content increases and then drops sharply when EPR content reaches 30 wt%. Thus in micro domains, the concentrations of polypropylene chain segments in blends increase with the increase of EPR content but they are lower than that in neat HPP. This phenomenon indicates the increasing nucleation ability with the increase of EPR content except HPP/EPR/E*b*P (60/30/10). During the cooling course, the easier nucleation allows longer segmental chains participating in molecule arrangement at higher temperatures, resulting in thicker lamellae.

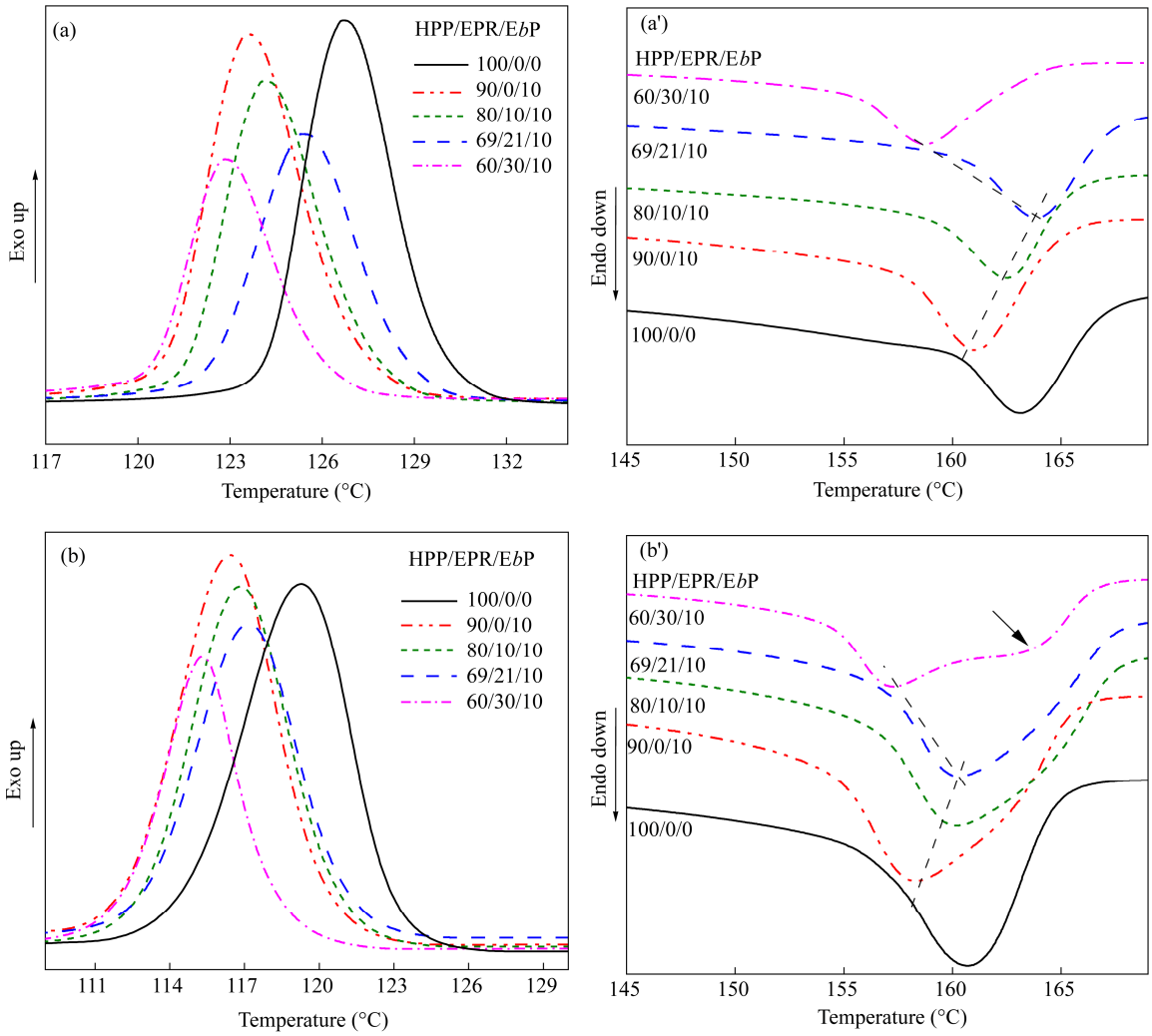


Fig. 5 DSC exotherms (a) (b) and endotherms (a') (b') under non-isothermal crystallization with cooling rates of 2 K/min (a) and 10 K/min (b) separately and heating rate of 10 K/min (a') (b')

At the cooling rate of 2 K/min, the difference in crystallization behavior is more obvious due to the amplified nucleating effect. Corresponding melting behavior reveals a similar composition dependence with isothermal crystallized samples. The melting peak indicated by the arrow in Fig. 5(b') results from recrystallization of imperfect crystals formed under faster cooling process.

The anomalous cases in all crystallization and melt peak temperatures appear for HPP/EPR/E*b*P (60/30/10) which may be ascribed to its special phase structure. The depressive compatibility and excessive EPR lead to an obvious network-like structure consisted of EPR-rich and HPP-rich phases and in turn eliminate the possible nucleation effect induced from EPR component.

Crystalline Structure

Figure 6 gives WAXD patterns for ternary blend samples. The diffraction angles at 14.0, 16.8, 18.6, 21.2 and 21.9 are corresponding to the (110), (040), (130), (111) and (131) lattice planes respectively, which mainly results from the α-monoclinic crystal of HPP[44]. As the most preferential direction, the diffraction of (110) lattice planes manifests marked contrast in diffraction intensity and peak width while other peaks show little difference. It means that the grain sizes of crystals on most lattice planes are similar except (110) lattice plane. Note that grain size of crystal is the normal thickness on lattice plane of lamella, which reflects growth of lamella along with the folding direction[45]. WAXD provides a very simple tool for estimating average size of the crystals (D) from the broadening of reflections by Scherrer equation[46]:

$$D = \frac{K\lambda}{\beta \cos\theta} \tag{2}$$

where K is the coefficient factor depending on geometry of crystallites (K = 0.89 for most crystalline polymers), λ is wavelength of the X-ray beam, β is the half width of diffraction peak (convert to radian before calculation) and θ is the angle of the considered Bragg reflection.

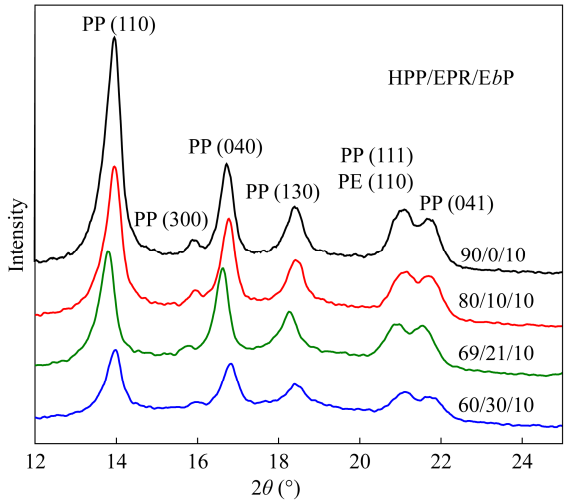


Fig. 6 WAXD patterns for HPP/EPR/E*b*P blends

The grain sizes of crystals based on (110) lattice plane are listed in Table 2. It can be found that D_{110} increases with the increase of EPR content, indicating the preferential growth along (110) lattice plane, which is in agreement with previous reports about PP/EPR blends[47, 48]. It is interesting that the variation trend of crystal size is similar to that of lamellar thickness for blends. It is noticed that they are actually measured in different directions. The lamellar thickness reflects the length of folding chains while the grain size of crystal is measured in growing direction. Besides, they are influenced by different factors. As mentioned above, the lamellar thickness (L_c) is related to nucleation as it is influenced by thickening time. And crystal size D lies on folding ability of chains in micro domains. The worse compatibility decreases the dispersion of EPR in HPP-rich phase with the increase of EPR content. As a result, the inhibition on chains folding in HPP-rich domain weakens. A direct correlation exists between crystal size D and surface free energy for folding. The larger the surface free energy for folding is, the more difficultly the chains fold and thicken along folding direction. The relationship

would be further discussed through a kinetic analysis on the basis of modified Lauritzen-Hoffman secondary nucleation theory.

Crystallization Kinetics of Blends

To further understand the crystallization behavior of ternary blends, Fig. 7 shows the isothermal growth rate G obtained from POM observations. It can be seen that the growth rates of blends are very close, especially at higher temperatures. A slight difference could be observed at low temperatures: growth rate G first increases and then turns down for HPP/EPR/E*b*P (60/30/10), with the increase of EPR content. Meanwhile, the overall crystallization rate G^*, characterized by $t_{1/2}$ from DSC data, presents a similar trend with growth rate G, as shown in Fig. 7. But smaller value of $t_{1/2}$ only means shorter time required to complete crystallization, rather than a sign of regularly folding ability for polymer chains. Unlike slight difference among G, the difference among G^* is distinct under the same condition. When the samples present a faster overall crystallization rate and similar growth rate at the same time, the deviation should result from enhanced nucleation behavior. In this situation, the primary nucleation behavior has a greater influence on the whole crystallization time.

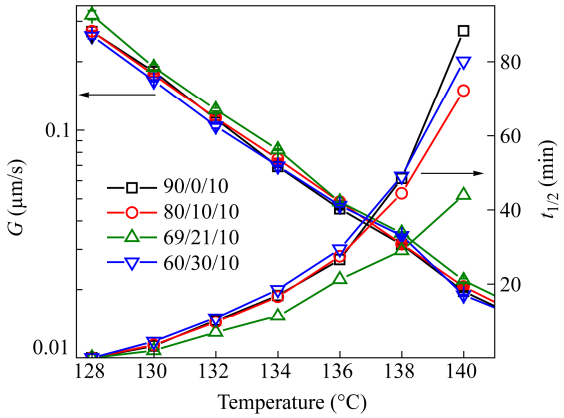


Fig. 7 Growth rates (G) and half crystallization times ($t_{1/2}$) of samples for isothermal crystallization at different temperatures

In order to quantitatively understand the effect of composition on crystallization behavior, a modified Lauritzen-Hoffman secondary nucleation theory[49] for polymer blends was applied to examine the crystallization kinetics. The isothermal growth rate G can be expressed by the classical equation:

$$\ln G - \ln \varphi_2 + \left[\frac{U^*}{R(T_c - T_\infty)}\right] - \frac{0.2T_m^0 \ln \varphi_2}{\Delta T} = \ln G_0 - \frac{K_g}{T_c(\Delta T)f} \tag{3}$$

where G_0 is a pre-factor, φ_2 is the volume fraction of the crystallizable component for HPP, and U^* is activation energy required for the transport of crystallizing segments across interphase, assigned a universal value of 6280 J/mol. R, the universal gas constant, equals to 8.31451 J/(mol·K); T_c is crystallization temperature and $T_\infty = T_g - 30$ K, is the temperature when transport ceases; T_g is the glass-transition temperature of HPP, with a value of −10 °C; $\Delta T = T_m^0 - T_c$, is the degree of supercooling; $f = 2T_c/(T_m^0 + T_c)$, is a correction factor accounting for reduction in latent heat of fusion when the temperature drops. And K_g, is the secondary nucleation exponent in a given regime. The K_g can be determined from the slope of plotting of $\ln G - \ln\varphi_2 + U^*/R(T_c - T_\infty) - 0.2T_m^0 \ln\varphi_2/\Delta T$ to $1/(T_c(\Delta T)f)$, according to Eq. (3) (Fig. 8).

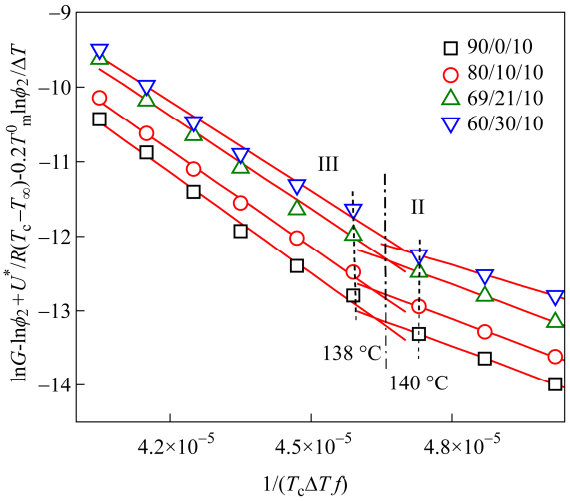


Fig. 8 Kinetic analysis of isothermal crystallization for HPP/EPR/E*b*P blends by a modified Lauritzen-Hoffman model (The regime II/III transition occurs at about 139 °C in this work.)

In addition, according to Hoffman's nucleation theory[49], K_g can be described as following:

$$K_g = \frac{nb_0\sigma\sigma_e T_m^0}{k\Delta h_f} \tag{4}$$

where b_0 = 0.626 nm is the thickness of chain stem, σ and σ_e are the free energy for lateral surface and folding surface separately (Here σ is 9.76 erg/cm^2 and is independent of the growth mode), and k is the Boltzmann constant (1.381 × 10^{-16} erg/K). In particular, n is a variable dependent on crystallization regime. The value of n is 4 in regimes I and III while it equals to 2 in Regime II. Regime I occurs typically at low undercooling where the secondary nucleation rate (i) is much less than the lateral substrate growing rate (g). When i increases to the same order of magnitude as g with increasing degree of undercooling, it is designated as regime II. In regime III, i becomes much larger than g[49, 50]. In addition, the σ_e can be obtained according to Eq. (4). All related parameters of crystallization kinetics are listed in Table 3.

Table 3. Parameters for isothermal crystallization kinetics of HPP/EPR/E*b*P blends

Samples	K_g(III) × 10^{-5} K^2 (128–140 °C)	σ_e(III) (erg/cm^2)	K_g(II) × 10^{-5} K^2 (140–144 °C)	σ_e(II) (erg/cm^2)	K_g(III)/K_g(II)
90/0/10	4.49	90.35	2.35	94.57	1.9
80/10/10	4.34	87.33	2.33	93.77	1.9
69/21/10	4.17	83.91	2.33	93.77	1.8
60/30/10	4.00	80.49	1.90	76.46	2.1

As seen in Fig. 8, the plot of each blend is divided into two linear parts. The results in Table 3 indicate that the ratio of the slopes at two adjacent temperature ranges is close to 2, completely conforming to Hoffman's Nucleation Theory. It locates at regime II when the temperature is over 140 °C and regime II /III transition occurs at about 139 °C (K_g(III)/K_g(II) = 2). The result is well consistent with the literature[51]. The calculated results show that the values of K_g and σ_e at both regimes decrease with increasing EPR content. Smaller value of K_g means the decreasing barrier for chain segments transferring to nucleus on the crystal growth front while small σ_e facilitates to regular folding of molecule chains. As they govern the formation and development of a new lamella separately, the great values of K_g and σ_e are unfavorable for the growth of crystals. Considering that the G slightly increases with increasing EPR content first and then turns down for HPP/EPR/E*b*P (60/30/10) blend, a good correspondence between G and σ_e appears, except blend with excessive EPR component of HPP/EPR/E*b*P (60/30/10). Given that growth rate G is an average parameter in macro-scale, it is determined not

only by the concentration of HPP in matrix in micro-scale but also by phase morphology in macro-scale. And σ_e is a parameter in micro-scale which could describe lamellar crystal. It affects the grain size of crystal in growing direction. The calculated results in Table 2 verify this deduction. As to HPP/EPR/E*b*P (60/30/10) blend, worse compatibility results in bad dispersion and an obviously bicontinuous phase structure consisting of EPR-rich and HPP-rich phases appears. The continuous network of EPR-rich phase limits the HPP phase in micro domain. In those domains, it is easy for crystallizable chains to fold with high HPP concentration. However, it is hard for crystal growth frontier to get across non-crystallizable phase of EPR.

Usually, after generation of critical crystal nuclei at early stage, multiple secondary nucleation and crystal growth events induce new lamellae at different surfaces[52, 53]. Hu *et al*.[52] asserted that the subsequent growth of polymer crystals was controlled by intramolecular nucleation on the growth front, which accounted for molecular segregation and was independent of the free energy barrier. Wunderlich *et al*.[53] referred to the secondary nucleation as the molecular nucleation, differing from primary crystal nucleation. Thus, secondary nucleation exponent K_g and surface free energy σ_e mainly describe process of subsequent crystal growth while primary nucleation is due to formation of critical crystal nuclei at an early stage, determined by phase morphology. In order to compare primary nucleation behavior, nucleation density of spherulite for various samples isothermally crystallized at 140 °C is exhibited in Fig. 9. It can be confirmed that the number of nuclei is almost constant in whole crystallization course, indicating a main predetermined nucleation in these ternary blends. The dependence of nucleation density on composition is in good accordance with the above deduction: it increases with increasing EPR content and a reversion appears for the blend of HPP/EPR/E*b*P (60/30/10). It also suggests that although the composition can simultaneously affect nucleation and growth rate of spherulite in these ternary blends, the nucleation density plays a more important role in determining overall crystallization rate. The results are considerable that the nucleation abilities of these ternary blends are proportional to interfacial area which is determined by composition (Fig. 2), but the nucleation effect vanishes in case a bicontinuous structure forms. For HPP/EPR/E*b*P (60/30/10), the lowest concentration of E*b*P leads to a poor compatibility between EPR and HPP, consequently the blend presents bicontinuous structure and little nucleation effect. In a word, primary nucleation behavior determined by phase morphology plays a major role in overall crystallization rate while secondary nucleation exponent is inclined to affect growth rate.

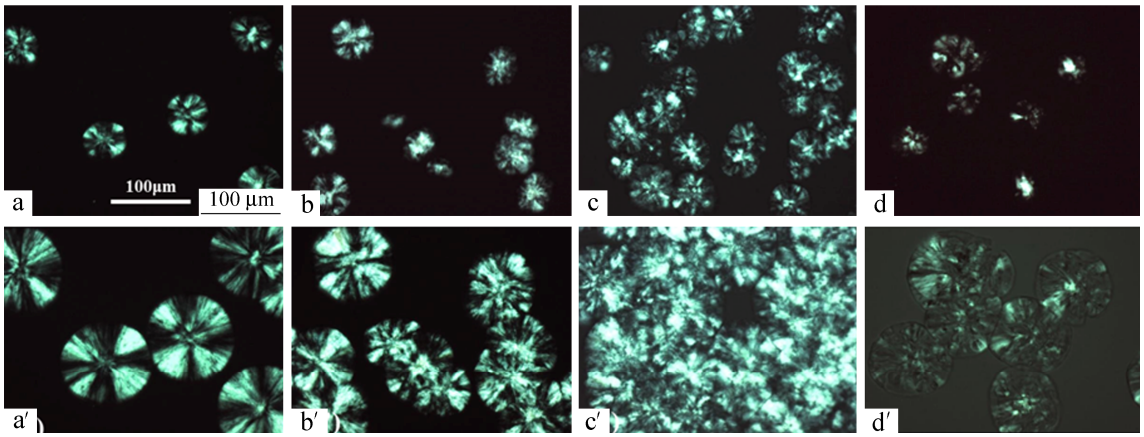


Fig. 9 POM images of HPP/EPR/E*b*P samples with different compositions: (a) (a') 90/0/10, (b) (b') 80/10/10, (c) (c') 69/21/10 and (d) (d') 60/30/10 during isothermal crystallization at 140 °C, at the 25 min (a)–(d) and 50 min (a')–(d') separately

CONCLUSIONS

To learn the compositional dependence of microstructure and crystallization behavior in IPC system, some HPP/EPR/E*b*P ternary blends with different compositions were prepared. When the EPR content in blend is no

more than 21 wt%, the dispersed phase occurs in core-shell structure. And the core-shell structure generally disappears and a bicontinuous phase structure forms in presence of 30 wt% EPR. Moreover, with the increase of amorphous EPR component, the interfacial area between domains increases so that the crystallization and melting behavior of ternary blend exhibit obvious composition dependence: (a) melting temperatures increase; (b) nucleation ability is enhanced while crystal growth is similar; (c) crystallization kinetics show a transition from regimes II to III occurring at about 139 °C, and the K_g and σ_e in both regimes decrease with increasing EPR content. However, all trends of behavior turn back for the composition of 60/30/10 as the content of amorphous phase reaches a critical value. These results are mainly ascribed to the different nucleation abilities induced by the compatibility. It is found that with the increase of EPR content, although the increased interfacial area and the decreased concentration of E*b*P lead to the worse compatibility between EPR and HPP, it facilitates to heterogeneous nucleation until the obvious bicontinuous phase structure appears.

REFERENCES

1 Zhu, H.J., Monrabal, B., Han, C.C. and Wang, D.J., Macromolecules, 2008, 41(3): 826
2 Nitta, K., Kawada, T., Yamahiro, M., Mori, H. and Terano, M., Polymer, 2000, 41(18): 6765
3 Tian, Y.F., Song, S.J., Feng, J.C. and Yi, J.J., Mater. Chem. Phys., 2012, 133: 893
4 Tan, H.S., Li, L., Chen, Z.N., Song, Y.H. and Zheng, Q., Polymer, 2005, 46(10): 3522
5 Zhang, C.H., Shangguan, Y.G., Chen, R.F., Wu, Y.Z., Chen, F., Zheng, Q. and Hu, G.H., Polymer, 2010, 51(21): 4969
6 Shangguan, Y.G., Zhang, C.H., Chen, R.F. and Zheng, Q.A., J. Appl. Polym. Sci., 2011, 119(3): 1560
7 Luo, F., Xu, C., Wang, K., Deng, H., Chen, F. and Fu, Q., Polymer, 2012, 53(8): 1783
8 Chen, R.F., Shangguan, Y.G., Zhang, C.H., Chen, F., Harkin-Jones, E. and Zheng, Q., Polymer, 2011, 52(13): 2956
9 Lin, Y., Chen, H.B., Chan, C.M. and Wu, J.S., Macromolecules, 2008, 41(23): 9204
10 Kojima, T., Kikuchi, Y. and Inoue, T., Polym. Eng. Sci., 1992, 32(24): 1863
11 Wu, S.H., Polym. Eng. Sci., 1990, 30(13): 753
12 Zheng, Q., Shangguan, Y.G. and Tao, L.Y., J. Appl. Polym. Sci., 2007, 106(1): 448
13 Shangguan, Y.G., Song, Y.H. and Zheng, Q., Polymer, 2007, 48(15): 4567
14 Kock, C., Gahleitner, M., Schausberger, A. and Ingolic, E., J. Appl. Polym. Sci., 2013, 128(3): 1484
15 Fu, Z.S., Tu, S.T. and Fan, Z.Q., Ind. Eng. Chem. Res., 2013, 52(17): 5887
16 Martuscelli, E., Pracella, M. and Wang, P.Y., Polymer, 1984, 25(8): 1097
17 Chen, J.Y., Cao, Y. and Li, H.L., J. Appl. Polym. Sci., 2010, 116(2): 1172
18 Martuscelli, E., Silvestre, C. and Abate, G., Polymer, 1982, 23(2): 229
19 Arroyo, M., Zitzumbo, R., and Avalos, F., Polymer, 2000, 41(16): 6351
20 Zheng, Q., Shangguan, Y.G., Yan, S.K., Song, Y.H., Peng, M. and Zhang, Q.B., Polymer, 2005, 46(9): 3163
21 Liu, Y.L., Xu, J.T., Dong, Q., Fu, Z.S. and Fan, Z.Q., Polym. Plast. Technol., 2009, 48(4): 333
22 Jin, J., Du, J., Chen, H.Y. and Han, C.C., Polymer, 2011, 52(26): 6161
23 Svoboda, P., Svobodova, D., Chiba, T. and Inoue, T., Eur. Polym. J., 2008, 44(2): 329
24 Tsuburaya, M. and Saito, H., Polymer, 2004, 45(3): 1027
25 Zhang, X.H., Man, X.K., Han, C.C. and Yan, D.D., Polymer, 2008, 49(9): 2368
26 Zhang, X.H., Wang, Z.G., Dong, X., Wang, D.J. and Han, C.C., J. Chem. Phys., 2006, 125(2): 024907
27 George, S., Varughese, K.T. and Thomas, S., Polymer, 2000, 41(14): 5485
28 Qiu, B.W., Chen, F., Lin, Y., Shangguan, Y.G. and Zheng, Q., Polymer, 2014, 55(23): 6176
29 Müller, A.J. and Arnal, M.L., Prog. Polym. Sci., 2005, 30(5): 559
30 Hansen, C.M., Prod. Res. Des., 1969, 8(1): 2
31 Song, S.J., Feng, J.C., Wu, P.Y. and Yang, Y.L., Macromolecules, 2009, 42(18): 7067
32 Chen, Y., Chen, Y., Chen, W. and Yang, D., J. Appl. Polym. Sci., 2008, 108(4): 2379
33 Thomson W., Philos. Mag. Ser., 1871,4(42): 448

34 Yamada, K., Hikosaka, M., Toda, A., Yamazaki, S. and Tagashira, K., Macromolecules, 2003, 36(13): 4790
35 Yamada, K., Hikosaka, M., Toda, A., Yamazaki, S. and Tagashira, K., Macromolecules, 2003, 36(13): 4802
36 Höhne, G.W.H., Polymer, 2002, 43(17): 4689
37 Cho, T.Y., Heck, B. and Strobl, G., Colloid Polym. Sci., 2004, 282(8): 825
38 Romanos, N.A. and Theodorou, D.N., Macromolecules, 2010, 43(12): 5455
39 Chen, J.H., Zhong, J.C., Cai, Y.H., Su, W.B. and Yang, Y.B., Polymer, 2007, 48(10): 2946
40 Hikosaka, M., Amano, K., Rastogi, S. and Keller, A., J. Mater. Sci., 2000, 35(20): 5157
41 Liu, Y.X., Li, J.F., Zhu, D.S., Chen, E.Q. and Zhang, H.D., Macromolecules, 2009, 42(8): 2886
42 Nurkhamidah, S. and Woo, E.M., Macromolecules, 2012, 45(7): 3094
43 Mezghani, K., Campbell, R.A. and Phillips, P.J., Macromolecules, 1994, 27(4): 997
44 Kakudo M. and Kasai M., "X-ray diffraction by polymers", Kodansha, Tokyo, 1972, p. 46
45 Hu. J.C., "X-ray Diffraction by Macromolecules", Science Press, Bei Jing, 2003, p. 150
46 Scherrer P, "Göttinger Nachrichten Math Phys", 1918, p. 98
47 Wang, L.X. and Huang, B.T., J. Polym. Sci. Polym. Phys., 1990, 28(6): 937
48 Shangguan Y.G., Zheng, Q. and Peng M., Acta Polymerica Sinica (in Chinese), 2005, (3): 389
49 Hoffman, J., Davis, G.T. and Lauritzen, J.J., "The Rate of Crystallization of Linear Polymers with Chain Folding" In: Hannay, N.B., editor. Treatise on Solid State Chemistry: Springer US, 1976, p. 497
50 Clark, E.J. and Hoffman, J.D., Macromolecules, 1984, 17(4): 878
51 Xu, J.N., Srinivas, S., Marand, H., and Agarwal, P., Macromolecules, 1998, 31(23): 8230
52 Hu, W.B., Frenkel, D. and Mathot, V.B.F., Macromolecules, 2003, 36(21): 8178
53 Wunderlich, B., Okazaki, I., Ishikiriyama, K. and Boller, A., Thermochim. Acta, 1998, 324(1–2): 77